Catalysis Letters, Vol. 116, Nos. 1–2, July 2007 (© 2007)
DOI: 10.1007/s10562-007-9090-0

A mesoporous oxidation catalyst La–Co–Ce–O prepared by citric acid complexation and organic template decomposition method

Jin-yong Luo,[a] Ming Meng,[a,*] Ying Qian,[a] Zhi-Qiang Zou,[a] Ya-ning Xie,[b] Tian-dou Hu,[b] Tao Liu,[b] and Jing Zhang,[b]

[a]*Department of Catalysis Science & Technology, School of Chemical Engineering and Technology, Tianjin University, Tianjin 300072, P.R. China*
[b]*Institute of High Energy Physics, Chinese Academy of Sciences, Beijing 100049, P.R. China*

Received 16 March 2007; accepted 16 March 2007

The mesoporous catalysts La–Co–Ce–O were successfully prepared in one step by citric acid complexation-organic template decomposition method, which show large surface area (up to 157 m^2/g), narrow pore diameter distribution (3.7∼3.9 nm), good thermal stability and high activity for CO and C_3H_8 oxidation. Based on the structural characterization results, it is found that the predominant Co phases are Co_3O_4 crystallites, and the activities of these mesoporous catalysts are not proportional to the amounts of surface cobalt atoms, but mainly related to the physical structure of the catalysts and the effective interaction between cobalt and cerium species. When the surface Co/Ce atomic ratio is close to 1, the catalytic synergy effect between them is maximized.

KEY WORDS: mesoporous catalyst; La–Ce–Co–O; citric acid complexation; total oxidation; structural characterization.

1. Introduction

Nowadays, almost all vehicles are equipped with three-way catalysts (TWCs) for the removal of the pollutants in the exhaust. However, during the cold start, these TWCs show very low efficiency for the oxidation of CO and HCs because of the low temperature of the catalyst-bed and exhaust itself [1]. Therefore, it is necessary to explore novel oxidation catalysts for the removal of CO and HCs at relatively low temperature.

It is reported that the cobalt oxides are excellent low-temperature oxidation catalysts, which can oxidize CO even at room temperature [2,3]. Lanthanum and cerium oxides are often added to the catalysts as promoters to improve the stability of the catalyst, the dispersion of the components, and to provide active oxygen species by a redox recycle between $Ce^{4+} \leftrightarrow Ce^{3+}$ [4,5]. So, it is a feasible idea to develop an oxidation catalyst containing La, Co and Ce. The most frequently reported La–Co–Ce–O catalysts are Ce-substituted $LaCoO_3$ perovskites or perovskite-like materials, which show good oxidation activity for hydrocarbon flameless combustion. Many preparation methods are developed to increase the surface area of these catalysts, like flame-hydrolysis [6], reactive grinding [7] and ZnO-improved complexation [8], since the larger surface area of the catalyst generally corresponds to the higher oxidation activity. Unfortunately, most of these catalysts show specific surface area not exceeding 30 m^2/g after calcination at 600 °C.

*To whom correspondence should be addressed.
E-mail: mengm@tju.edu.cn

In the last several years, much attention has been attracted to the mesoporous materials with large surface area and uniform pore diameter. But up to now, the most work mainly focuses on the synthesis of Si-containing molecular sieves, such as MCM-41, MCM-48 [9,10], which normally show no oxidation activity and just serve as supports. Based on the methods used for preparing mesoporous Si-containing molecular sieves, we have successfully prepared a series of mesoporous non-silica mixed oxide catalysts La–Co–Ce–O [11] and La–Co–Zr–O [12] using cetyltrimethyl ammonium bromide (CTAB) as the cationic template. These catalysts show excellent activities for the total oxidation of CO and C_3H_8, but the structure of the La–Co–Ce–O catalyst still remain unclear. In the present work, the techniques of nitrogen adsorption/desorption, XRD, XPS, EXAFS, TPR were used for the careful structural characterization of the La–Co–Ce–O catalysts, and the correlation between the catalyst structure and the catalytic performance is demonstrated in detail.

2. Experimental

2.1. Catalyst preparation

All the reagents are of analytical purity grade and have been received from Tianjin Chemical Reagent Co., Inc. The procedure for catalyst preparation has been described in detail in a previously study [11]. In brief, an amorphous La–Co citrate complex precursor, prepared by dissolving hydrated lanthanum, cobalt nitrate (the La/Co atomic ratio was fixed at 1) and citric acid in

distilled water, and the other two solutions of CTAB and hydrated cerium nitrate were mixed to give a clear homogenous solution. Then 2 M NaOH was quickly added to this solution to form a gel at a pH of 11 ± 0.5. After stirring for 6 h, this gel was hydrothermally condensed at 95 °C for 48 h. The solid product was filtered, washed with ethanol, dried overnight at 110 °C and finally calcined in air at different temperatures for 4 h. These samples are denoted as LCC(x)−y, where x and y represent the atomic ratio of (La + Co)/(La + Co + Ce) and the calcination temperature (centigrade), respectively. For comparison, a La–Co–Ce–O mixed oxide with the composition of $x = 0.5$ was prepared by the conventional co-precipitation method, namely by adding 2 M NaOH to the solution containing hydrated lanthanum, cobalt and cerium nitrate at a pH of 11 ± 0.5, the obtained solid was washed with water, dried at 120 °C and calcined at 500 °C, which is denoted as LCC(0.5)-CP-500.

2.2. Catalyst characterization

XRD powder diffraction patterns were recorded on a RIGAKU D/Max-2500 diffractometer with a rotating copper anode using Cu Kα_1 radiation ($\lambda = 1.5405$ Å) as X-ray source. The data of 2θ from 20 to 80° were collected with the stepsize of 0.02 °.

Surface area, pore volume and pore size distribution were measured by nitrogen adsorption/desorption at 77 K using a Thermo-Finnigan SORPTOMATIC 1990 apparatus. The samples were degassed at 320 °C for 8 h prior to the adsorption experiments. The surface area (S_{BET}) was determined by the BET method in the 0.0893–0.2970 partial pressure range and the pore size distribution was determined by the Barrett-Joyner-Halenda (BJH) method from the desorption branch of the isotherm.

Temperature programmed reduction (H_2-TPR) measurement was performed on a Thermo-Finnigan TPDRO 1100 instrument with a thermal conductivity detector (TCD). The reducing gas contains 5 vol% H_2 balanced by pure N_2, and a flow rate of 20 ml/min was used. The quartz tube reactor was loaded with 30 mg sample in powder form and heated from 30 °C to 900 °C at a rate of 10 °C /min.

X-ray photoelectron spectra (XPS) were recorded with a PHI-1600 ESCA spectrometer using Mg-Kα radiation (1653.6 eV). The base pressure was 5×10^{-8} Pa. The binding energies were calibrated using C1s peak of contaminant carbon (B.E. = 284.6 eV) as standard. The surface composition of the samples in terms of atomic ratios was calculated, using a Shirley-type background and empirical cross-section factors for XPS.

Extended X-ray absorption fine structure (EXAFS) measurements were carried out on the 1W1B beamline of Beijing Synchrotron Radiation Facility (BSRF) operating at about 80 mA and 2.2 GeV. The absorption spectra of the Co K-edge of samples and reference materials were recorded at room temperature in transmission mode. A Si (111) double-crystal monochromator was used to reduce the harmonic content of the monochrome beam. The back-subtracted EXAFS function was converted into k space and weighted by k^3 in order to compensate for the diminishing amplitude due to the decay of the photoelectron wave. The Fourier transforming of the k^3-weighted EXAFS data was performed in the range $k = 3.4$ to 12.4 A^{-1} with a Bessal window.

2.3. Evaluation of catalytic activity

Catalyst evaluation was carried out in a continuous fixed-bed quartz tubular reactor (i.d. 8 mm) mounted in a tube furnace. The temperature was measured both outside and inside the catalyst bed. The feed and product mixtures were analyzed by a gas chromatograph (BFS SP-3430) equipped with a thermal conductivity detector and a flame ionization detector. For CO oxidation, the feed gas mixture contains CO (1.1 vol%) and O_2 (3 vol%), while for C_3H_8 oxidation, it contains C_3H_8 (0.85 vol%) and O_2 (10 vol%), using pure N_2 as balance gas. The gas hourly space velocities (GHSV) for CO and C_3H_8 oxidation are 18 000 h^{-1} and 12 000 h^{-1}, respectively.

3. Results and discussion

3.1. Texture data from nitrogen adsoption/desorption

The nitrogen adsorption/desorption isotherm of the sample LCC(0.5)-500 is shown in figure 1(a), which exhibits a typical type IV shape [13]. The P/P_0 position of the inflection point corresponds to a diameter in the mesoporous range, and the BJH pore size distribution is narrowly centered at about 3.9 nm, indicating a uniform pore size distribution in this sample. Even calcined at 600 °C, this uniform mesoporous structure is still maintained as seen in figure 1 (b), suggesting the good thermal stability of these mixed oxides. The other two samples with different atomic ratios also show similar pore size distributions, indicating the effectiveness of this method for the preparation of the uniform mesoporous mixed oxide catalysts.

The texture data of the samples are summarized in table 1. All the samples calcined below 600 °C exhibit large surface area (S_{BET}) above 100 m^2/g, among which the LCC(0.5)-400 sample shows the highest surface area of 157 m^2/g. After calcination at 500 °C, this mixed oxide still has a large surface area of 130 m^2/g, presenting a striking contrast to the sample LCC(0.5)-CP-500 by co-precipitation method with only a specific surface area of 24 m^2/g. After calcination at 600 °C, this sample still has a satisfactory surface area of 95 m^2/g.

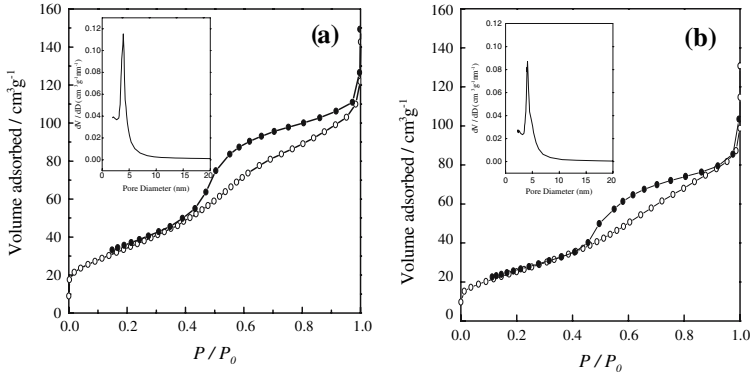

Figure 1. Nitrogen adsorption/desorption isotherms of the La–Co–Ce–O catalysts (a) LCC(0.5)-500; (b) LCC(0.5)-600 (Insert: BJH pore diameter distribution).

Table 1
Specific surface area and pore texture data of LCC(x)-y catalysts

Sample	S_{BET} (m^2g^{-1})	Pore volume (cm^3g^{-1})	Pore diameter (nm)
LCC(0.3)-500	112	0.168	0.372
LCC(0.7)-500	108	0.184	0.393
LCC(0.5)-400	157	0.175	0.388
LCC(0.5)-500	130	0.168	0.391
LCC(0.5)-600	95	0.135	0.395
LCC(0.5)-800	22	0.064	–

While the mesopores in these materials have collapsed after calcination at 800 °C, as suggested by the great decrease in the surface area and the pore volume for the LCC(0.5)-800 sample (see table 1).

3.2. XRD

The XRD patterns of the samples LCC(0.5)-y and the sample LCC(0.5)-CP-500 are shown in figure 2(a). All samples clearly display the diffraction peaks corresponding to CeO_2 and Co_3O_4 [14]. Compared with the sample prepared by the coprecipitation method, the diffraction peaks for the sample by organic template decomposition method are rather broad and weak, indicating the smaller crystallites and higher component dispersion in these samples. It is also found that with the increase of calcination temperature, the diffraction peaks of CeO_2 are intensified obviously, while those of the Co_3O_4 show very limited increase in the intensity. Worth noting that no $LaCoO_3$ phase is detected (disappearance of the characteristic diffraction peak at 23 ° for $LaCoO_3$, [8]) and Co_3O_4 is still the main cobalt-containing phase even calcined at 800°C, suggesting the excellent thermal stability of Co_3O_4 crystallites. Normally, the temperature of 800 °C is high enough for the $LaCoO_3$ perovskite formation. On the one hand, the isolation effect of the template has decreased the opportunities for all the three kinds of La, Co and Ce species to simultaneously assemble together on molecular scale, after the removal of the template (below 400 °C), the independent oxide phases of La, Co and Ce may have formed, which are more difficult to reform the perovskite phase even at higher temperature, such as 800 °C. On the other hand, after calcination at 800 °C, the sample LCC(0.5)-800 still remains a specific surface area as high as 22 m^2/g, in such situation, even if a small amount of perovsike phase had formed, it would be

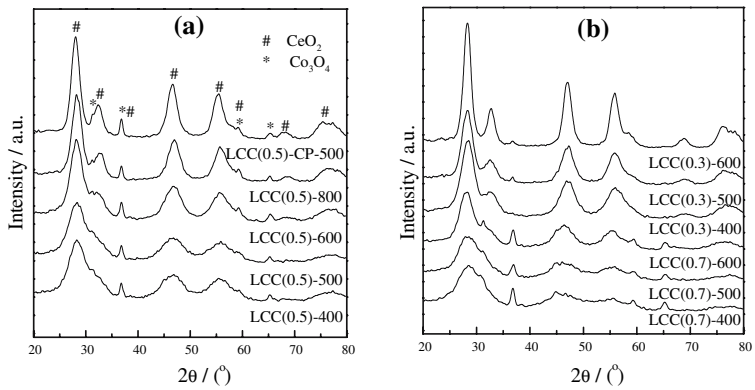

Figure 2. XRD patterns of the La–Co–Ce–O catalysts: (a) LCC(0.5)-y (b) LCC(x)-y.

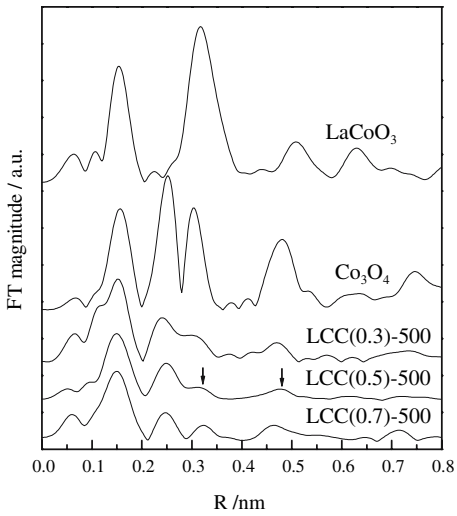

Figure 3. RSFs of Co K-edge of the samples.

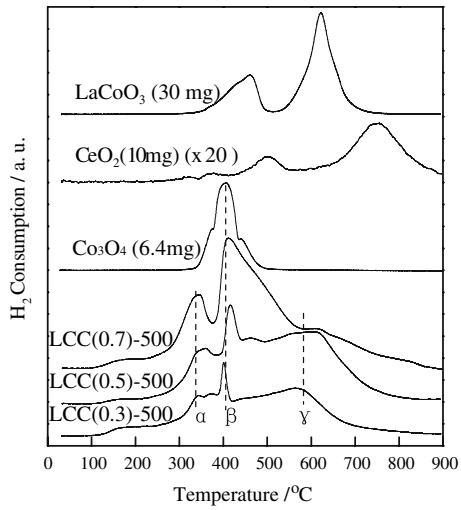

Figure 4. TPR profiles of LCC(x)-500.

difficult to be detected by XRD due to its high dispersion and small amount.

3.3. EXAFS

Figure 3 shows the radial structural functions (RSFs) of the Co K-edge for Co_3O_4, $LaCoO_3$ and LCC(x)-500 samples from EXAFS. Pure Co_3O_4 shows mainly four peaks at 0.157 nm, 0.250 nm, 0.303 nm and 0.480 nm (not corrected by phase scattering shift). The first peak represents the nearest Co-O coordination shells with one third of Co (Co^{2+}) tetrahedrally coordinated at 0.181 nm and other two thirds (Co^{3+}) octahedrally coordinated at 0.199 nm. These two shells are too near to be separated in the RSF. The second and third peaks correspond to the Co-Co coordination shell at 0.287 nm (Coordination Number, CN: 4) and 0.335 nm (CN: 8), while the fourth peak should be attributed to the higher Co-Co and Co-O shells [15]. For $LaCoO_3$, its RSF just shows two major peaks at 0.154 nm and 0.317 nm, corresponding to the octahedrally coordinated Co-O shell at 0.193 nm and higher Co-La, Co-Co and Co-O shells between 0.330 nm and 0.39 nm, respectively [16]. Compared with the standard samples, the RSFs of the samples resemble the pure Co_3O_4, especially in the occurrence of the second coordination peak at 0.250 nm, which does not exist in pure $LaCoO_3$. Thus it is deduced that the Co species are mainly present as Co_3O_4 phase. This is in good agreement with XRD results where Co_3O_4 is the only detected Co-containing phase. From the view of peak intensity, it is easily found that the peaks of the samples are much weaker than pure Co_3O_4, implying the high dispersion state of Co species in these samples. Generally, the intensity of the peaks corresponding to the high coordination shells provides an indication of the crystallization degree of the corresponding metal or oxides [17,18]. Note that the third peak at ~ 0.30 nm and the fourth peak at ~ 0.48 nm for sample LCC (0.5)-500 are weaker than those of the other two samples, suggesting that the Co_3O_4 phase in this sample has the highest dispersion.

3.4. TPR

TPR tests were carried out in order to determine the nature of the cobalt species. Figure 4 shows the TPR profiles for the La–Co–Ce–O samples with different atomic ratios, as well as the pure CeO_2 and Co_3O_4. All the samples prepared by organic template decomposition method have three major reduction peaks, labeled as α, β and γ, with the peak maximum at about 340 °C, 410 °C and 586 °C, respectively. These peaks are mainly related to the reduction of Co species due to the much higher reducibility of Co species compared with cerium and lanthanum oxides.

The reduction patterns for Co_3O_4 are rather controversial in literature. Bruce [19] and Ernst [20] reported the reduction of Co_3O_4 is a two-stage process, involving in reduction to CoO. Simonot [21] observed a single reduction peak during Co_3O_4 TPR test. Spadaro [22] concluded that the appearance of the $Co_3O_4 \rightarrow CoO \rightarrow Co^0$ reduction steps depends strongly on the experimental conditions, catalyst composition and dispersion behavior. Generally, transition metal oxides, like CuO get reduced in a wider temperature range by a two-step stage when contacting with ceria [23,24]. The first reduction step is always promoted by the interaction between them while the second step is delayed by the stabilization effect of ceria on the cations at the medium valence. On this basis, the assignment is therefore made as follow:

Peak α: reduction of the highly dispersed and/or small crystallite Co_3O_4 phase interacting with CeO_2 to CoO;
Peak β (sharp): reduction of the XRD-visible, well defined crystalline Co_3O_4 particles to metal Co;

Peak γ: reduction of the Co^{2+} interacting with CeO_2 to Co^0.

The highest intensity of peak γ in the sample LCC(0.5) is indicative of the largest amount of the Co species interacting with CeO_2. This is consistent with the EXAFS results. According to EXAFS, Co_3O_4 phase in this sample has the highest dispersion, thus the contact probability between Co and CeO_2 is promoted, which results in the largest amounts of Co species interacting with CeO_2. This enhanced contact may have a great influence on the catalytic activity, which will be discussed in the following section.

3.5. XPS

All the Co species of these samples display a main peak for Co2p3/2 at 779.4 eV (figure not shown). The 2p3/2 and 2p1/2 spin-orbit value is about 15.2 eV. Such results are the typical characteristics of Co_3O_4 [25], consistent with the findings from XRD and EXAFS analysis.

In terms of surface atomic ratios in table 2, it can be seen that the percentage of the Co atoms is always larger and that of Ce atoms always smaller than the bulk composition, indicating surface Co enrichment and Ce deficiency. It is worth noting that the surface composition of Co and Ce varies significantly from samples with different bulk composition, while La just displays few changes. For the surface Co/Ce atomic ratios, these samples make a great difference, they are 1.0, 0.3 and 4.5 for the samples LCC(0.5)-500, LCC(0.3)-500 and LCC(0.7)-500, respectively. The Co/Ce ratio is closely related to the catalytic activity, which is discussed in the next section.

3.6. The activity for CO and C_3H_8 oxidation

The light-off temperatures for the oxidation of CO and C_3H_8 on the ternary La–Co–Ce oxides are shown in figure 5. It can be seen that the samples prepared by the organic template decomposition method are much more active than that by co-precipitation method for both CO and C_3H_8 oxidation. Compared with sample LCC(0.5)-CP-500, the temperatures T_{90} of sample LCC(0.5)-500 for CO and C_3H_8 oxidation are decreased by 30 °C and 55 °C, respectively. From the XRD and nitrogen adsorption/desorption characterization results, it can be inferred that the prominent difference in the oxidation ability is due to the following two aspects: (1) The sample prepared by the organic template decomposition method have larger specific surface area and higher component dispersion, leading to much more exposed active sites for the catalytic reaction. (2) The efficiency for the utilization of the inner surface is increased by the uniform mesoporous structure, which facilitates the diffusion and transportation of the reactants, and makes it easier for the contact between the reactants and the active sites. All these catalysts also show appreciable stability towards the oxidation reactions without drop of the activity in at least 4 h. When this sample is calcined at 800 °C, the surface area is obviously decreased and the uniform mesopores collapsed, leading to the great decrease in oxidation ability.

Table 2
The XPS results of LCC(x)-500 samples

Sample	Binding Energy (eV)			Surface Atomic (%)		
	$Co2p_{3/2}$	$La3d_{5/2}$	$Ce3d_{5/2}$	La	Co	Ce
LCC(0.3)-500	779.4	833.3	881.6	21.0	17.7	61.3
LCC(0.5)-500	779.3	833.6	881.8	26.2	36.8	36.9
LCC(0.7)-500	779.4	833.8	881.8	23.5	62.7	13.9

For CO oxidation, as compared with noble metal catalysts (mainly Pt and Pd), LCC(0.5)-500 catalyst shows higher activity because these noble metals are self-poisoned by the strong CO adsorption at low temperature [26]. Table 3 lists the catalytic performance of some noble metal (Pt and Pd-based) catalysts for C_3H_8 oxidation in terms of light-off temperatures T_{50} and T_{90}. From this table, it can be seen that the mesoporous mixed oxide La–Co–Ce–O is of comparable activity to those noble metal catalysts. In view of the limited resources and high prices of noble metals, these mesoporous oxides possess obvious advantages.

Now, a question still remaining is that, why the samples with (La + Co/La + Co + Ce) ratio of 0.5 always show the best activity for both CO and C_3H_8 oxidation, even if the loading of Co is not the highest. Compared with LCC(0.3)-500 and LCC(0.7)-500, the T_{50} temperature of LCC(0.5)-500 for CO oxidation decreases by 24 °C and 30 °C, and the T_{90} for C_3H_8 oxidation decreases by 17 °C and 30 °C, respectively. Thus the order of activity is not consistent with the surface cobalt concentration. The EXAFS and TPR characterization results show that the Co_3O_4 in the LCC(0.5)-500 has the highest dispersion, which will exert a substantial influence on the surface composition. According to the XPS analysis, the LCC(0.5)-500 possesses a surface Co/Ce ratio close to 1, but this ratio sharply increases to 4.5 for LCC(0.7)-500 and decreases to 0.3 for LCC(0.3)-500. It seems that neither the surface Co nor the surface Ce enrichment that contributes to the high oxidation ability, but a proper surface Co/Ce ratio plays an essential role for the catalytic oxidation process. The close amounts of the surface Co and Ce atoms may increase the contact probability and maximize the catalytic synergism between Co and Ce phases. It has been calculated by Shapovalov [28] that the M–O (M = Au, Ag, Cu) bond distance in doped ceria is much larger than the distance between the dopant and the oxygen in the dopant's own oxide, and our previous study over the highly dispersed $CuO/CeO_2–Al_2O_3$ catalyst has

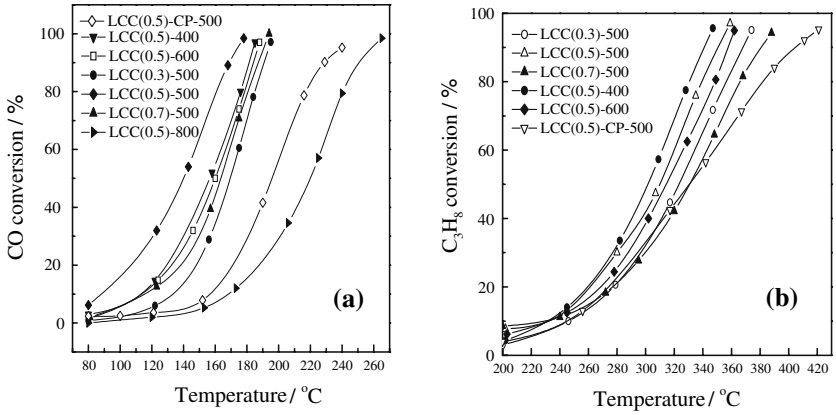

Figure 5. Light-off curves for (a) CO oxidation (b) C_3H_8 oxidation.

Table 3
The catalytic performance of various catalysts towards C_3H_8 total oxidation

Catalyst	T_{50}/°C	T_{90}/°C	Experimental conditions	Ref.
CK306[a]	338	388	0.5% C_3H_8 /10%O_2/Ar, SV[b] = 242 $cm^3\ g^{-1}\ min^{-1}$	[27]
0.3 wt% Pd/TGF[c]	360	400	0.5% C_3H_8 /10%O_2/Ar, SV = 242 $cm^3\ g^{-1}min^{-1}$	[27]
0.2 wt% Pt/TGF	290	420	0.5% C_3H_8 /10%O_2/Ar, SV = 242 $cm^3\ g^{-1}min^{-1}$	[27]
$La_{0.5}Co_{0.5}CeO_x$	301	341	0.85% C_3H_8 /10%O_2/N_2, SV = 250 $cm^3\ g^{-1}min^{-1}$	this work

[a]industrial granulated catalyst; [b]space velocity; [c]titania modified glass fiber.

evidenced the increase in the Cu-O bond length by EXAFS characterization [29]. Considering the similarity of these transition metals, the synergetic interaction between cobalt and cerium may weaken the surface Co–O bond by increasing the bond distance, which will promote the bond activation and the oxygen transferring during CO oxidation.

4. Conclusions

(1) The mesoporous La–Co–Ce mixed oxides were successfully prepared in one step by citric acid complexation-organic template decomposition method using CTAB as template. These mesoporous catalysts possess high specific surface areas (up to 157 m^2/g), very uniform pore diameters (3.7∼3.9 nm) and good thermal stability (up to 600 °C).
(2) The structural characterization results of XRD, XPS and Co K-edge EXAFS show that the cobalt species predominantly exist as Co_3O_4 phase. But two types of cobalt species exist, namely the highly dispersed and/or small crystallite Co_3O_4 interacting with the CeO_2 as well as the well defined XRD-visible crystalline Co_3O_4.
(3) These mesoporous materials exhibit excellent activities for CO and C_3H_8 total oxidation, and could be comparable to the noble metal-based (Pt, Pd) catalysts. The catalytic oxidation activities are not proportional to the amount of surface cobalt atoms, but closely related to physical aspects like the surface area and the pore structure, as well as the chemical aspects. The large surface area increases the number of exposed active sites and the uniform mesopores facilitate the mass transfer rate, while the synergetic interaction between cobalt and cerium may promote the activation of Co–O bond by increasing the surface Co–O distance. This synergism is maximized when the surface Co/Ce atomic ratio is close to 1.

Acknowledgments

This work is financially supported by the National Natural Science Foundation of China (No. 20676097), the National Hi-Tech Research & Development Program (“863” Project) of China (No. 2006AA06Z348), the Natural Science Foundation of Tianjin of China (No. 05YFJMJC09700) and the Specialized Research Fund for the Doctoral Program of Higher Education of China (No. 20040056028).

References

[1] R. Westerholm, A. Christensen and A. Rosen, Atmos. Environ. 30 (1996) 3529.
[2] S. Colonna, S. De Rossi, M. Faticanti, I. Pettiti and P. Porta, J. Mol. Catal. A 180 (2002) 161.

[3] J. Jansson, A.E.C. Palmqvist, E. Fridell, M. Skoglundh, L. Osterlund, P. Thormahlen and V. Langer, J. Catal. 200 (2002) 387.
[4] S.J. Schmieg and D.N. Belton, Appl. Catal. B 6 (1995) 127.
[5] A. Bueno-Lopez, K. Krishna, M. Makkee and J.A. Moulijn, J. Catal. 230 (2005) 237.
[6] R. Leanza, I. Rossetti, L. Fabbrini, C. Oliva and L. Forni, Appl. Catal. B 28 (2000) 55.
[7] V. Szabo, M. Bassir, A. Van Neste and S. Kaliaguine, Appl. Catal. B 37 (2002) L175.
[8] J. Shu and S. Kaliaguine, Appl. Catal. B 16 (1998) L303.
[9] K. Chauhari, T.K. Das, A.J. Chandwadkar and S. Sivasanker, J. Catal. 186 (1999) 81.
[10] K. Chauhari, R. Bal, A.J. Chandwadkar and S. Sivasanker, J. Mol. Catal. 177 (2002) 247.
[11] J.Y. Luo, M. Meng, Y. Qian and Y.Q. Zha, Chin. J. Catal. 27 (2006) 471.
[12] Z.Q. Zou, M. Meng, J.Y. Luo, Y.Q. Zha, Y.N. Xie, T.D. Hu and T. Liu, J. Mol. Catal. 249 (2006) 240.
[13] K.S.W. Sing, D.H. Everett, R.A.W. Haul, L. Moscou, R.A. Pierotti, J. Rouquerol and T. Siemieniewska, Pure Appl. Chem. 57 (1985) 603.
[14] L.F. Liotta, G. Di Carlo, G. Pantaleo and G. Deganello, Catal. Commun. 6 (2005) 329.
[15] G.P. Huffman, N. Shah, J. Zhao, F.E. Huggins, T.E. Hoost, S. Halvorsen and G. Goodwin Jr., J. Catal. 151 (1995) 17.
[16] O. Haas, R.P.W.J. Struis and J.M. McBreen, J. Solid State Chem. 177 (2004) 1000.
[17] O.V. Komova, A.V. Simakov, V.A. Rogov, D.I. Kochubei, G.A. Odegova, V.V. Kriventsov, E.A. Paukshtis, V.A. Ushakov, N.N. Sazonova and T.A. Nikoro, J. Mol. Catal. A 161 (2000) 191.
[18] J.R. Chang, S.L. Chang and T.B. Lin, J. Catal. 169 (1997) 338.
[19] L.A. Bruce, M. Hoang, A.E. Hughes and T.W. Turney, Appl. Catal. A 100 (1993) 51.
[20] B. Ernst, L. Hilaire and A. Kiennemann, Catal. Today 50 (1999) 413.
[21] L. Simonot, F. Garin and G. Maire, Appl. Catal. B 11 (1997) 167.
[22] L. Spadaro, F. Arena, M.L. Granados, M. Ojeda, J.L.G. Fierro and F. Frusteri, J. Catal. 234 (2005) 451.
[23] A. Martinez-Aris, M. Fernandez-Garcia, O. Galvez, J.M. Coronado, J.A. Anderson, J.C. Conesa and G. Munuera, J. Catal. 195 (2000) 207.
[24] M. Fernadez-Garcia, E.G. Rebollo, A.G. Ruiz, J.C. Conesa and J. Soria, J. Catal. 172 (1997) 146.
[25] D.V. Cesar, C.A. Perez, M. Schmal and V.M.M. Salim, Appl. Surf. Sci. 157 (2000) 159.
[26] U. Oran and D. Uner, Appl. Catal. B 54 (2004) 183.
[27] L. Kiwi-Minsker, I. Yuranov, E. Slavinskaia, V. Zaikovskii and A. Renken, Catal. Today 59 (2000) 61.
[28] V. Shapovalov and H. Metiu, J. Catal. 245 (2007) 205.
[29] J.Y. Luo, M. Meng, Y.Q. Zha, B. He and S.Q. Wei, Chinese J. Inorg. Chem. 22 (2006) 861.